The International Journal of Advanced Manufacturing Technology (2023) 124:4159–4173
https://doi.org/10.1007/s00170-022-09383-x

ORIGINAL ARTICLE

A kinematic precision reliability evaluation method for rotor-bearing systems considering multi-source wear degradations and random errors

Hongwei Wang[1] · Jiawei Xiang[1] · Xufeng Zhao[2] · Yulong Li[3]

Received: 17 April 2022 / Accepted: 16 May 2022 / Published online: 25 May 2022

Abstract
Rotor-bearing systems play a vital role in machine tools, aero engines, and wind turbines. Generally, worn-induced degradation quantities and manufacturing errors of components are the main error sources that influence the precision reliability of rotor-bearing systems. The current precision reliability evaluation models are focusing on several error sources in only a few key components without agreeable results. Therefore, a precision reliability evaluation model is proposed considering all time-variant error sources and random error sources. Firstly, time-variant wear models for commonly occurred degradation types in a rotor-bearing system are developed. Secondly, the constructed time-variant wear models are inserted into the precision model with all moving components in the rotor-bearing system using meta-action structural decomposition method. Finally, the time-variant stochastic process discretization method is employed to establish the precision reliability evaluation model, and solve the precision reliability of the rotor-bearing systems. Case investigations are carried out to verify the performance of the present model, which provides a more accurate precision reliability evaluation model to estimate the conditions of rotor-bearing systems during the service period.

Keywords Rotor-bearing systems · Precision reliability evaluation · Time-variant wear models · Random error sources · Meta-action

1 Introduction

Rotor-bearing systems are widely used in the transmission process of mechanical movement and momentum. The performances of rotor-bearing systems need to meet different requirements in different application scenarios. Thereby, the performance design has always been the dominant issue in the stage of system development design. The randomness and time variability of kinematic precision can be expressed by a reliability index [1]. The precision reliability can be earmarked as an important constraint index in the research on tolerance allocation [2], and it is also an important basis for formulating maintenance strategy [3]. Consequently, it is necessary to establish a kinematic precision reliability evaluation method with more accurate performance for rotor-bearing systems to serve the precision design.

An effective and correct precision expression model plays an important role in the research of kinematic precision reliability. In recent years, much attention has been paid to the aspect of the precision modeling theories for rotor-bearing systems. Tang et al. [4] introduced the stream of variation theory into geometric error modeling for mechanical systems, regarded each moving component as a station, and calculated the accumulated geometric errors according to the transmission sequence from the upstream station to the downstream station. Yang and Ding [5] represented the error propagation process from one component to the other different component with a differential motion matrix, and built the integrated precision model of the whole kinematics chain by homogeneous transformation matrices. Bozca [6] calculated the transmission precision of the gear system based on

✉ Jiawei Xiang
wxw8627@163.com

[1] School of Mechanical and Electrical Engineering, Wenzhou University, Wenzhou 325035, People's Republic of China

[2] College of Economics and Management, Nanjing University of Aeronautics and Astronautics, Nanjing 210016, People's Republic of China

[3] School of Mechanical Engineering, Yangzhou University, Yangzhou 225127, People's Republic of China

a state-space model. Liu et al. [7] regarded the error accumulation between components as the screw motion of rigid bodies, and established the precision model of systems by screw theory and Jacobian function. Yang et al. [8] established a six-degree-of-freedom geometric motion errors model of the precision rotary stage by adopting the rigid body hypothesis and the spatial transformation matrix. Wang et al. [9] proposed a transmission error model of the ball screw by converting manufacturing errors and installation errors to the errors in normal and axial direction. However, the assembly precision caused by the geometric errors of components and the transmission precision caused by the relative motion relationship of kinematic pairs are not distinguished in the current precision modeling methods, which cannot reflect the motion essence of mechanical systems. Moreover, there are various error sources for the complex system with many components which lead to the cumbersome calculation process and inaccurate results. The main cause of this problem is that the error sources are not reasonably classified in the traditional structured decomposition method. From the perspective of motion modularization, meta-action theory [10] produces a reasonable balance in the subordinate relationship between components and systems. And some applications in reliability analysis have been carried out [11]; the advantages in failure mode and effects analysis have also been proved [12, 13]. Mu et al. [14] introduced the application of meta-action theory in the remaining useful life prediction on account of its advantage in the reflection of the interaction among the components. Chen et al. [15] applied meta-action theory for the reliability optimization design of mechanical systems. Yang et al. [16] presented a performance degradation prediction approach by combining meta-action theory with the digital twin technology. Xiao et al. [17] further explored the motion modularization strategy of the meta-action unit, which can reflect the characteristics of the mechanical systems that the function determined by the motion. Therefore, meta-action theory also lay a good foundation for the precision modeling.

The random geometric errors of components caused by the uncertainty of the manufacturing process are considered as the initial error sources affecting the precision reliability of rotor-bearing systems, and some meaningful research work on the analysis of such errors has been proposed. Huang et al. [18] considered the original manufacturing errors of gears as the random variables affecting the transmission error of the gear mechanism, and presented a kinematic accuracy reliability analysis method using the saddle-point approximation technique. Cai et al. [19] established a geometric/kinematic error model for mechanical systems using homogenous transformation matrices, regarded the geometric error values as random quantities within the tolerance range, and developed an accuracy reliability analysis model based on the high-order moment standardization technique. Wang et al. [20] estimated the probability distribution of the precision state function for mechanical systems with random geometric errors based on the statistical fourth moment method, and employed the Edgeworth series to analyze the dynamic precision reliability. Zhang et al. [21] conducted the importance sampling method to analyze the accuracy reliability of mechanical systems after establishing a comprehensive error model affected by the random geometric errors. Yang et al. [22] analyzed the error propagation between parts based on small displacement torsor and multi-tolerance coupling, presented the assembly precision model of mechanical rotating systems in accordance with the Jacobian-torsor method, and calculated the assembly precision reliability according to the probability distribution of the assembly error index. Ma et al. [23] performed the effects of the stochastic rotor/stator gap caused by manufacturing on vibrational behaviors and reliability of the rotor systems. In addition, there are some time-variant error sources such as the wears on gears and bearings during the operation of the rotor-bearing systems. Wang et al. [24] calculated the wear depths of the parts by the Archard wear model, considered the part geometric parameters in the wear formula as input random variables, and constructed the Kriging models to predict the time-variant reliability of mechanical systems. Chen et al. [25] decomposed the time-varying dynamic transmission error of the gear mechanism into many random variables according to the meshing period, thus realizing the transformation of a time-dependent reliability solution into a time-independent reliability solution, and estimated the reliability based on the saddle-point approximation method. Jiang et al. [26] calculated the cumulative wear of gears in the gear transmission system and the meshing force and stress distribution under the influence of gear wear, and predicted the system dynamic reliability according to the gear strength degradation rule. Furthermore, stochastic models [27] can also be used to describe the process of performance degradation, such as the gamma process model [28] and the Wiener process model [29], and the precision reliability evaluation using the PHI2 method [30], support vector machine [31], response surface method [32], and the Kriging method [33] have been reported in literature. Unfortunately, to the best of our current knowledge, there are few reports in literature which have combined the manufacturing error sources with the time-variant wear sources to evaluate the effects on the kinematic precision reliability of rotor-bearing systems, and that leads to many important error items being ignored and the inaccuracy model.

Motivated by the above-mentioned limitations, a novel kinematic precision reliability modeling method is proposed to improve the accuracy of reliability assessment for rotor-bearing systems in this paper. Specifically, based on the meta-action structural decomposition method, the precision analysis model containing each source related to the output precision of rotor-bearing systems is established. When the distribution

of random errors and the expression of time-variant wears are determined, the kinematic precision reliability can be calculated by the time-variant stochastic process discretization method. The remainder of this manuscript is organized as follows: Sect. 2 provides the time-varying wear models for the probably worn components in rotor-bearing systems. In Sect. 3, the output precision model based on the meta-action structural decomposition method is established. Section 4 presents the precision reliability evaluation model considering multi-source wear degradations and random errors. The applicative case is reported in Sect. 5 to validate the proposed method. The conclusions are finally drawn in the final section.

2 Time-variant wear models

The precision time variation and failure of rotor-bearing systems are primarily caused by the wearing of components, especially the wear occurring on gears and bearings. Therefore, these two types of wear are analyzed specifically and respectively as follows.

2.1 Tooth thickness wear

Tooth thickness wear is the gear material continuous reduction process under stress. The wear quantity of the tooth profile surface at a certain time can be calculated by the Archard model. Let V represent the wear volume of the tooth surface and s the relative sliding distance; then

$$\frac{V}{s} = k\frac{W}{H} \tag{1}$$

where k is the wear coefficient, W the normal pressure on the contact surface, and H the hardness of the material.

By discretizing the contact area on the tooth surface into several contact points, the infinitesimal wear quantity of the arbitrary contact point at a certain time can be obtained and calculated as

$$\delta h = \int_0^s \frac{kP}{H} ds \tag{2}$$

where P represents the contact stress at the contact point.

The wear coefficient k is a parameter comprehensively affected by factors such as working condition, surface roughness, lubrication characteristics, and material characteristics. According to the Janakiraman regression formula [34], it can be calculated as

$$k = \frac{3.981 \times 10^{29}}{E_e} L^{1.219} G^{-7.377} S^{1.589} \tag{3}$$

And $L = \frac{W\prime}{E_e R_e}$, $G = \alpha_0 E_e$, $S = \frac{\sqrt{R_{a1}^2 + R_{a2}^2}}{R_e}$.

Where equivalent elastic modulus $E_e = 1 \Big/ \left(\frac{1-v_{(1)}^2}{E_{(1)}} + \frac{1-v_{(2)}^2}{E_{(2)}} \right)$ and $v_{(1)}$, $v_{(2)}$ and $E_{(1)}$, $E_{(2)}$ are Poisson ratio and elastic modulus of the driving and driven wheel's material, respectively. $W\prime$ is the load per unit length. Equivalent radius of curvature $R_e = 1 \Big/ \left(\frac{1}{r_{b(1)}} + \frac{1}{r_{b(2)}} \right)$, $r_{b(1)}$, and $r_{b(2)}$ are the base circle radius of the driving and driven wheel, respectively. α_0 is the pressure-viscosity coefficient of lubricating oil (assuming it is a constant not affected by pressure during the wearing process). $R_{\alpha 1}$ and $R_{\alpha 2}$ are the roughness of these two contact surfaces, respectively.

According to Hertz contact theory, the contact stress P can be solved by taking the tooth surface meshing problem of the driving and driven gear equivalent to the mutual extrusion problem of two cylinders. When these two tooth surfaces are in line contact under stress, a rectangular contact area is formed due to elastic deformation. The contact stress distribution of a certain cross section in the contact area at a certain time is shown in Fig. 1.where $P_{\max}$ represents the maximum Hertz contact stress. Half width of Hertz contact area $a = \sqrt{\frac{4W\prime R_e}{\pi E_e}}$ and the variation range of the relative sliding distance s is $[0, a]$.

As demonstrated in Fig. 1, the maximum contact stress occurs in the center of the contact area and has a decaying trend to both sides. Contact stress at the arbitrary contact point is calculated as

$$P(x) = \frac{2P_{\max}}{\pi a^2} \sqrt{\left(a^2 - x^2\right)} \tag{4}$$

where the maximum contact stress $P_{\max} = T_{(1)} \big/ B_{(1)} r_{b(1)} \cdot T_{(1)}$ is the load transmitted by the gear pair; $B_{(1)}$ is the tooth width of the driving gear. Therefore, the calculation equation of the single infinitesimal wear quantity can be rewritten as

$$\delta h = \int_0^a \frac{2kT_{(1)}}{\pi a^2 B_{(1)} r_{b(1)} H} \sqrt{\left(a^2 - x^2\right)} dx \tag{5}$$

When the driving wheel rotates once, the contact point of the tooth surface completes single wear accumulation, while the driven wheel completes the corresponding number of times of wear accumulations due to the relationship of the

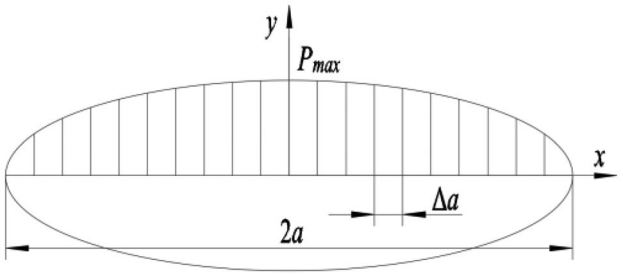

Fig. 1 Hertz contact stress distribution

transmission ratio. Therefore, the wear quantity of the driving gear tooth thickness can be calculated as

$$\Delta e_{g(1)}(t) = \delta h_{g(1)} \cdot n_{g(1)} \cdot t \tag{6}$$

The wear quantity of the driven gear tooth thickness can be calculated as

$$\Delta e_{g(2)}(t) = \delta h_{g(2)} \cdot n_{g(2)} \cdot t \tag{7}$$

2.2 Bearing wear

Rolling bearings are generally composed of rolling elements, bearing outer ring, locking inner ring, and bearing cage. The roller and the raceway move relative to each other in a point-contact manner. A single roller not only rotates around its own axis, but also rolls around the bearing axis on the raceway, and under the force of the bearing cage, the roller also slides on the raceway to a certain extent. Therefore, the internal friction of the rolling system is a compound friction including rolling and sliding friction.

To facilitate the analysis and calculation, it is assumed that the rolling elements are uniformly worn, that is, the wear loss of each roller at a certain time is the same. The rollers move independently, and there is no radial clearance between the rollers and the inner and outer rings. Similar to the calculation of tooth thickness wear, the continuous wear process of bearing is firstly discretized into several infinitesimal wearing moments. Assuming that the wear loss of each point on the contact line at each moment is the same, according to the Archard wear model, the infinitesimal wear loss of the contact point at a certain moment can be calculated as

$$\delta h = \int_0^t kPv_s dt \tag{8}$$

where k represents the material wear coefficient, and the calculation equation is the same as Eq. (3). P represents the contact stress at the contact point. v_s represents the relative sliding speed. dt is the infinitesimal contact time.

Normally, the rollers contact with the outer raceway due to the centrifugal force F_c. The force analysis of the roller is shown in Fig. 2. Considering that the rotation speed ω is small, the influence of centrifugal force can be ignored. where N_i represents the normal pressure exerted by the inner raceway on the rollers. N_o represents the support force of the outer raceway to the roller. F_k^1 and F_k^2 represent the force of the bearing cage. f_i and f_o represent the friction between the inner and outer raceways and the rollers, respectively.

According to Hertz contact stress distribution in Fig. 1, the half-width a of the contact area is discretized into m units with a width of $\Delta a = a/m$. Taking the contact between the inner raceway and the roller as an example, the calculation equation of the half width of the contact area $a^{(i,g)}$ is

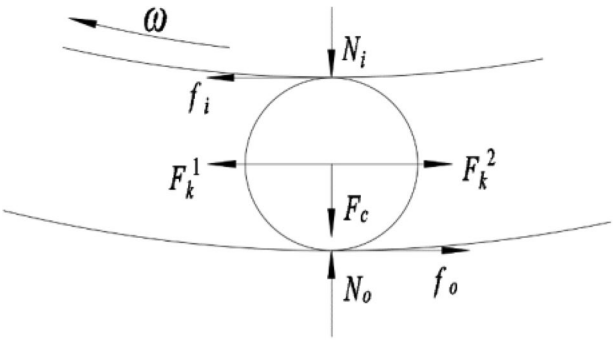

Fig. 2 Force analysis of the cylindrical roller in the load-bearing area

$$a^{(i,g)} = \sqrt{\frac{4W^{(i,g)}}{\pi}\left(\frac{1-\upsilon_i^2}{E_i} + \frac{1-\upsilon_g^2}{E_g}\right)\left(\frac{r_i r_g}{r_i + r_g}\right)} \tag{9}$$

where $W^{(i,g)}$ is the contact load. υ_i, υ_g and E_i, E_g are Poisson ratio and elastic modulus of the inner ring and roller material, respectively. r_i and r_g are the contact curvature radius of the inner raceway and the roller, respectively.

Considering that the effective meshing width is much smaller than the meshing length, when the contact area is discretized into units, the slight difference in the equivalent curvature radius between contact units is ignored. Thus, the normal contact stress of the k-th unit within the half width of each contact area can be obtained as

$$P_k^{(i,g)} = P_{\max} \times \sqrt{1 - \left(\frac{\Delta a^{(i,g)} \times k - \Delta a^{(i,g)}/2}{a^{(i,g)}}\right)} \tag{10}$$

Let R_i be the diameter of the inner raceway, R_o the diameter of the contact point of the outer raceway, R_g the diameter of the rollers, R_{or} the diameter of the bearing rollers' center circle, $\vartheta = R_g/R_{or}$, and n the rotational speed of the inner ring, and let the angular velocity of the inner ring and the worm gear be kept the same. Then, the revolution angular velocity of rollers is calculated as

$$\omega_g^R = \frac{1}{2}\omega(1-\vartheta) \tag{11}$$

The rotation angular velocity of rollers is calculated as

$$\omega_g^r = \frac{R_{or}}{2R_g}\omega(1+\vartheta)(1-\vartheta) \tag{12}$$

Since the inner ring rotates and the outer ring remains stationary during the motion of the rolling bearing, there are two pairs of friction pairs in the bearing, so the wear value of the bearing includes three parts: the outer ring, the inner ring, and the rollers. The wear values of the inner and outer rings are determined by the single wear value

and the number of rolling contact at a contact point in one revolution cycle. The bearing including z rollers, when the inner ring of the bearing makes one rotation on its axis,

$$N_i = \frac{\omega - \omega_g^R}{\omega} \times z = \frac{z}{2}(1+\vartheta) \tag{13}$$

The number of rollers in contact with the outer raceway is

$$N_o = \frac{\omega_g^R}{\omega} \times z = \frac{z}{2}(1-\vartheta) \tag{14}$$

Therefore, the calculation equation of the wear quantity of the contact point on the inner raceway is obtained as

$$\delta h_i = a^{(i,g)} \cdot z \cdot (1+\vartheta) \cdot n \cdot t \cdot \sum_k^m \left[k_k^{(i,g)}\left(P_k^{(i,g)}\right) \cdot P_k^{(i,g)} \right] \tag{15}$$

The calculation equation of the wear quantity of the contact point on the outer raceway is obtained as

$$\delta h_o = a^{(o,g)} \cdot z \cdot (1-\vartheta) \cdot n \cdot t \cdot \sum_k^m \left[k_k^{(o,g)}\left(P_k^{(o,g)}\right) \cdot P_k^{(o,g)} \right] \tag{16}$$

For the roller, its revolution speed is $n_g^R = \frac{1}{2}n(1-\vartheta)$. Since the roller is in contact with both the inner and outer raceways during one rotation, the calculation equation of the wear quantity of the contact point on the roller can be obtained as

$$\begin{aligned} \delta h_g &= a^{(i,g)} \cdot \frac{n_g^r}{n_g^R} \cdot n \cdot t \cdot \sum_k^m \left[k_k^{(i,g)}\left(P_k^{(i,g)}\right) \cdot P_k^{(i,g)} \right] + a^{(o,g)} \cdot \frac{n_g^r}{n_g^R} \cdot n \cdot t \cdot \sum_k^m \left[k_k^{(o,g)}\left(P_k^{(o,g)}\right) \cdot P_k^{(o,g)} \right] \\ &= \frac{R_{or}}{R_g} \cdot (1+\vartheta) \cdot n \cdot t \cdot \left\{ a^{(i,g)} \cdot \sum_k^m \left[k_k^{(i,g)}\left(P_k^{(i,g)}\right) \cdot P_k^{(i,g)} \right] + a^{(o,g)} \cdot \sum_k^m \left[k_k^{(o,g)}\left(P_k^{(o,g)}\right) \cdot P_k^{(o,g)} \right] \right\} \end{aligned} \tag{17}$$

Finally, the total wear volume of the bearing $\Delta e_r(t)$ is calculated as

$$\begin{aligned} \Delta e_r(t) = \delta h_i + \delta h_o + \delta h_g &= a^{(i,g)} \cdot \left(z + \frac{R_{or}}{R_g} \right) \cdot (1+\vartheta) \cdot n \cdot t \cdot \sum_k^m \left[k_k^{(i,g)}\left(P_k^{(i,g)}\right) \cdot P_k^{(i,g)} \right] \\ &+ a^{(o,g)} \cdot \left[z \cdot (1-\vartheta) + \frac{R_{or}}{R_g} \cdot (1+\vartheta) \right] \cdot n \cdot t \cdot \sum_k^m \left[k_k^{(o,g)}\left(P_k^{(o,g)}\right) \cdot P_k^{(o,g)} \right] \end{aligned} \tag{18}$$

3 Output kinematic precision model based on meta-action structural decomposition

The performance of rotor-bearing systems is often presented as multiple indicators, and the essential factors that form and affect these indicators are the geometric characteristics of the components. Traditional precision modeling often leads to imprecise model expression due to the large number of components, and cannot consider all the error terms that affect the motion. The meta-action unit (MAU) is a structural unit composed of the moving part and other related components that ensure its correct action. Meta-action theory finds a reasonable balance between the dependencies of components and systems. Most of the components that compose the meta-action unit are assembled in a fixed connection, and its movement is mainly accomplished by plane or cylindrical contact. To solve the relationship between indicators and geometric error items, the accumulation geometric error of intra-MAU and transmission kinematic precision of inter-MAU are calculated separately.

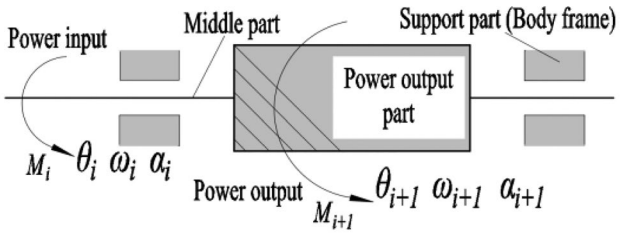

Fig. 3 Rotation meta-action unit

3.1 Meta-action basic concepts

The meta-action unit refers to the most basic form of motion in mechanical products which can accomplish motion and power transmission. The most common forms of motion in mechanical systems are the rotary motion around the fixed axis and the linear motion along the mating surface. Therefore, these two motions are defined as rotation and translation MAU, respectively. Rotor-bearing systems are composed of rotation MAUs.

M represents the transmission torque, θ the output angular displacement, ω the angular velocity, and α the angular acceleration, as shown in Fig. 3.

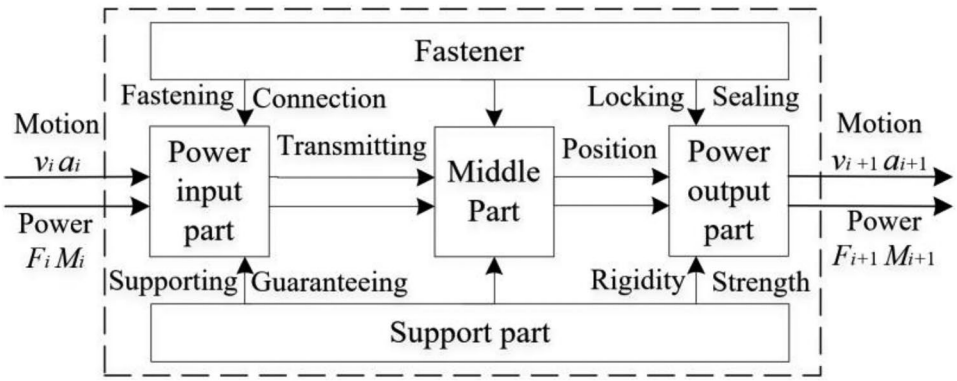

Fig. 4 Structural conceptual model of the meta-action unit

MAU is the smallest granularity to accomplish an action, and the most basic structural unit that transmits motion and power in mechanical products. As is shown in Fig. 4, MAU consists of a power input part, middle parts, fasteners, support parts, and a power output part. The power input part provides the power source or receives the output power of the upper MAU, such as gears and screws. The role of the middle parts is to transmit motion and ensure the correct position of the power input and output parts, such as connecting keys, rotating shafts, locating pins, bearings, and bushings. Fasteners play the role of connection, tightening, anti-loosening, and sealing, such as screws, springs, sealing rings, and end caps. The boxes and bases are generally taken as the support parts. The power output part is used as the end movement or power output.

3.2 Spatial pose of the power output part in MAU

The essence of MAU is to ensure that the power output part completes the designed motion. In order to achieve the expected motion trajectory, the position and orientation errors of the power output part in the X, Y, Z, α, β, and γ directions in the space coordinate system need to be within the specified error range, and the geometric errors of the power input and output parts. The spatial error of the power output part is the accumulation result of machining errors, assembly errors, and wear of the components in MAU. During the assembly process of MAU, the actual pose of the power output part is offset relative to the ideal pose in the X, Y, Z, α, β, and γ directions in the space coordinate system, as shown in Fig. 5.

The screw theory is used to calculate the accumulation error between the parts in MAU. When the arbitrary point in the space coordinate system rotates around a unit vector $\boldsymbol{\omega}$ by an angle θ, its rotation matrix can be calculated according to Rodrigues' rotation equation as

$$e^{\theta\widehat{\omega}} = \mathbf{E} + \widehat{\boldsymbol{\omega}} \sin\theta + \widehat{\boldsymbol{\omega}}^2(1-\cos\theta) \tag{19}$$

where the antisymmetric matrix $\widehat{\boldsymbol{\omega}} = \begin{pmatrix} 0 & -\omega_z & \omega_y \\ \omega_z & 0 & -\omega_x \\ -\omega_y & \omega_x & 0 \end{pmatrix}$.

The motion of the arbitrary rigid body in the space coordinate system can be regarded as a spiral motion around a certain vector axis. The screw-exponential product form of its coordinate change is expressed as

$$\mathbf{g} = \begin{pmatrix} e^{\theta\widehat{\omega}} & (\mathbf{E} - e^{\theta\widehat{\omega}})(\boldsymbol{\omega}\times\boldsymbol{v}) + \theta\boldsymbol{\omega}\boldsymbol{\omega}^T\boldsymbol{v} \\ 0 & 1 \end{pmatrix} \tag{20}$$

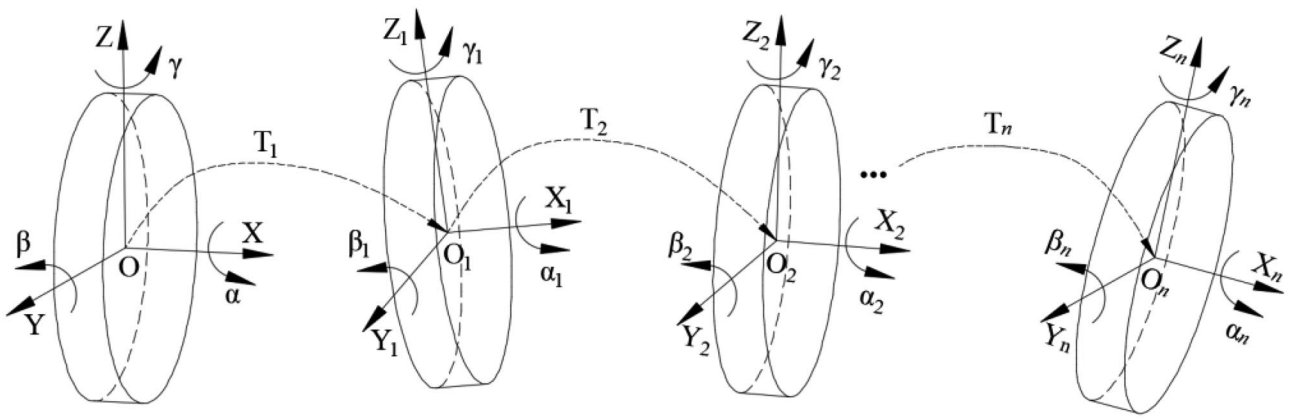

Fig. 5 Space pose formation process of the power output part

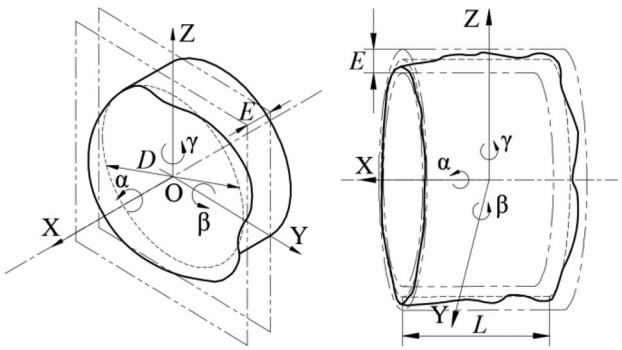

a. Plane fit **b.** Cylindrical fit

Fig. 6 Two fit forms in rotor-bearing systems

where $\boldsymbol{\nu}$ represents the displacement vector moving along the vector axis.

The pose change of the power output part in the space coordinate system can be decomposed into the spiral motion around the X, Y, and Z directions, and further decomposed into the movement $\delta_i (i = x, y, z)$ and rotation $\varepsilon_j (j = x, y, z)$ around the X, Y, and Z axes. Considering that the error amount is infinitesimal relative to the geometric size of the part, let $\sin \varepsilon_i = \varepsilon_i$, $\cos \varepsilon_i = 1$ and ignore the high-order infinitesimal. Then, according to Eq. (20), the pose change screw expression of the power output part is obtained as

$$\mathbf{g}^o = \prod_{\substack{i=x,y,z \\ i=x,y,z}} \mathbf{g}_{\delta_i} \mathbf{g}_{\varepsilon_j} = \begin{pmatrix} 1 & -\varepsilon_z & \varepsilon_y & \delta_x \\ \varepsilon_z & 1 & -\varepsilon_x & \delta_y \\ -\varepsilon_y & \varepsilon_x & 1 & \delta_z \\ 0 & 0 & 0 & 1 \end{pmatrix} \tag{21}$$

The basic fit forms in rotor-bearing systems include plane fit and cylindrical fit, which are shown in Fig. 6.

As shown in Fig. 6a, the plane fit constrains three degrees of freedom in the X, β, and γ directions, so errors in these three directions are also generated. Assuming that all parts in MAU are rigid bodies, and their contact is a rigid fit, the spatial errors of plane fit during the assembly process are represented by homogeneous coordinate transformation as

$$\mathbf{g}_p^o = \begin{pmatrix} 1 & -\varepsilon_z & \varepsilon_y & \delta_x \\ \varepsilon_z & 1 & 0 & 0 \\ -\varepsilon_y & 0 & 1 & 0 \\ 0 & 0 & 0 & 1 \end{pmatrix} \tag{22}$$

where $\delta_x \approx \frac{E}{2}$, $\varepsilon_y \approx \frac{E}{D}$, and $\varepsilon_z \approx \frac{E}{D}$. D represents the diameter of the rotating shaft and E represents the error value.

As is shown in Fig. 6b, the plane fit constrains four degrees of freedom in the Y, Z, β, and γ directions, so errors in these four directions are also generated. The spatial errors of cylindrical fit during the assembly process are represented by homogeneous coordinate transformation as

$$\mathbf{g}_c^o = \begin{pmatrix} 1 & -\varepsilon_z & \varepsilon_y & 0 \\ \varepsilon_z & 1 & 0 & \delta_y \\ -\varepsilon_y & 0 & 1 & \delta_z \\ 0 & 0 & 0 & 1 \end{pmatrix} \tag{23}$$

where $\delta_y \approx \frac{E}{2}$, $\delta_z \approx \frac{E}{2}$, $\varepsilon_y \approx \frac{E}{L}$, and $\varepsilon_z \approx \frac{E}{L}$. L represent the length of the rotating shaft and E represents the error value.

The spatial pose of the power output part is determined by the geometric errors $\mathbf{g}_i^o (i = 1, 2, \ldots, n)$. The error expression model of the power output part after assembly is

$$\mathbf{g}_m = \prod_{i}^{n} \mathbf{g}_i^o \tag{24}$$

3.3 Output precision of MAU chain

According to the principle of freedom degree, the function of a MAU chain is generally accomplished by series structures. The MAU chain transmits power from the input end to the output end in the motion transmission direction (Fig. 7). Few rotor systems with redundant structures or dual driving structures are beyond the scope of this paper.

There are several motion precision indicators, such as indexing precision, repositioning precision, and radial runout, which are used to characterize the performance of the motion transmitted by the MAU chain. These indicators are obtained through the accumulation of the error components in each direction, which are caused by the spatial pose of the power output part and the geometric characteristics of the power input and output part. In this paper, the indexing precision reliability is selected as the performance evaluation index. Indexing precision is determined by the tooth profile error, tooth thickness error, and eccentricity errors of the power input and output parts. And the eccentricity errors include the assembly error component of the power output part in the direction perpendicular to the rotation axis.

The tooth profile error refers to the normal distance between the two tooth profile lines with the smallest distance within the tooth width effective range on a given section (Fig. 8). The tooth profile error is approximately equivalent

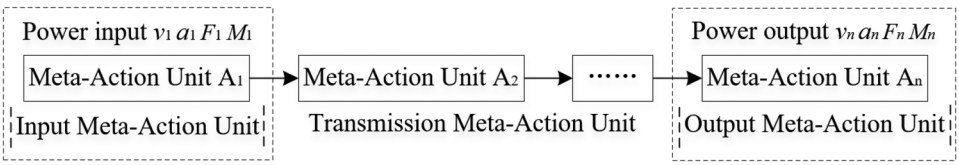

Fig. 7 The structural model of the MAU chain

to a harmonic function of the tooth-to-tooth and total tangential composite errors.

Let the gear meshing frequency be ω_m and the gear rotation frequency be ω_s; then, the tooth profile error is calculated as

$$\Delta e_s = 0.5\Delta f_{ic}^{'} \sin(2\pi\omega_m t) + 0.5\Delta F_{ic}^{'} \sin(2\pi\omega_s t) \tag{25}$$

Let the initial tooth thickness error of the power input part in MAU be Δe_{ig}^{I}, the tooth thickness wear be $\Delta e_{g}^{I}(t)$, the tooth profile deviation be Δe_{s}^{I}, and the eccentricity error caused by the accumulated assembly error be Δe_{ip}^{I}. Angular velocity is ω_m^I, pressure angle is α. And initial phase angle β^I are random variables that obey uniform distribution in the interval $[0, 2\pi]$.

Let the initial tooth thickness error of the power output part in MAU be Δe_{ig}^{O}, the tooth thickness wear be $\Delta e_{g}^{O}(t)$, the tooth profile deviation be Δe_{s}^{O}, the eccentricity error caused by the accumulated assembly error be Δe_{ip}^{O}, and the eccentricity error caused by wear be $\Delta e_{p}^{O}(t)$. Angular velocity is ω_m^O, pressure angle is α. And initial phase angle β^O are random variables that obey uniform distribution in the interval $[0, 2\pi]$.

Then the indexing precision of MAU is obtained as

$$\begin{aligned}\Delta e_i(t)=&\Delta e_{ig}^{I} + \Delta e_{g}^{I}(t) + \Delta e_{s}^{I} + \Delta e_{ip}^{I} \sin\left(2\pi\omega_m^I t + \beta^I + \alpha\right) + \Delta e_{ig}^{O} + \Delta e_{g}^{O}(t) + \\ &\Delta e_{s}^{O} + \left(\Delta e_{ip}^{O} + \Delta e_{p}^{O}(t)\right) \sin\left(2\pi\omega_m^O t + \beta^O + \alpha\right)\end{aligned} \tag{26}$$

Assuming that the rotor-bearing system is composed of n MAUs, then the indexing precision of the rotor-bearing system can be obtained as

$$\Delta e(t) = \sum_{i}^{n} \Delta e_i(t) \tag{27}$$

4 The construction of kinematic precision reliability evaluation model

Assuming that the allowable indexing accuracy of rotor-bearing systems is Δe^*, the precision reliability function of rotor-bearing systems is built as

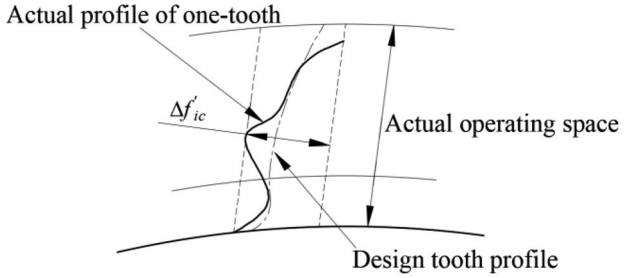

Fig. 8 One-tooth meshing error of the worm wheel

$$g(\boldsymbol{X}(t), \boldsymbol{Y}, t) = \sum_{i}^{n} \Delta e_i(t) - \Delta e^* \tag{28}$$

This function includes both the initial random error variables and the time-variant wear quantity. Stochastic process discretization is adopted to solve the time-variant reliability question. Firstly, the time-variant process in a certain time interval is discretized into many micro time units. When the discretization degree reaches a certain level and the influence of time variables on the output value is ignored, the error in a micro time unit approximately obeys a Gaussian distribution. In this way, the time-variant reliability problem is transformed into the random variable problem in traditional reliability research.

Assuming that the running time of a rotor-bearing system is $[0, T]$, the time interval is discretized into m equal micro time units with step length $\Delta t = \frac{T}{m}$. Then, the random process vector $\boldsymbol{X}(t) = \left(X_1(t), X_2(t), ..., X_n(t)\right)$ with n time-variant wear parameters is discretized as

$$\boldsymbol{X}_i = \left[\boldsymbol{X}_1(t_i), \boldsymbol{X}_2(t_i), ..., \boldsymbol{X}_n(t_i)\right]^T, i = 1, 2, ..., m \tag{29}$$

Thus, the kinematic precision reliability of rotor-bearing systems is expressed as [35]

$$P_s(T) = P\left\{\bigcap_{i=1}^{m}\left[g\left(\boldsymbol{X}_i, \boldsymbol{Y}, t_i\right) > 0, t_i = \left(i - \frac{1}{2}\right)\Delta t, \Delta t = \frac{T}{m}\right]\right\} \tag{30}$$

where $g\left(\boldsymbol{X}_i, \boldsymbol{Y}, t_i\right)$ is the random performance function discretized from the time-variant performance function $g(\boldsymbol{X}(t), \boldsymbol{Y}, t)$, and Y is an l-dimensional random vector independent of $\boldsymbol{X}(t)$.

Considering the correlation between the discrete random vectors, the parameters are converted into independent standard normal distributions before solving. Based on Nataf transform [36], the random vectors $\boldsymbol{X}_i$ and $\boldsymbol{Y}$ in Eq. (30) are converted into standard normal distribution vectors $\boldsymbol{U}_i$ and $\boldsymbol{V}$ as follows:

$$U_{i,k} = \Phi^{-1}\left(F_{X_{i,k}}\left(X_{i,k}\right)\right), i = 1, 2, ..., m; k = 1, 2, ..., n \tag{31}$$

$$V_p = \Phi^{-1}\left(F_{Y_p}\left(Y_p\right)\right), p = 1, 2, ..., l \tag{32}$$

where $\Phi^{-1}(\cdot)$ is the cumulative distribution inverse function of the standard normal distribution, and $F_{X_{i,k}}(\cdot)$ and $F_{Y_p}(\cdot)$ are the cumulative distribution functions of random vectors $\boldsymbol{X}_i$ and $\boldsymbol{Y}$, respectively.

Let $g^*\left(\boldsymbol{U}_i, \boldsymbol{V}, t_i\right)$ represent the transformed performance function of the random vectors $\boldsymbol{U}_i$ and $\boldsymbol{V}$; then, the most probable point of the function is solved as

$$\begin{cases} \min\left\|\left(\boldsymbol{U}_i^T, \boldsymbol{V}^T\right)^T\right\| \\ s.t. g^*\left(\boldsymbol{U}_i, \boldsymbol{V}, t_i\right) = 0 \end{cases} \tag{33}$$

Thus, the calculation equation of β_i, the i-th index value in the reliability index vector $\boldsymbol{\beta}$ corresponding to $g^*\left(\boldsymbol{U}_i, \boldsymbol{V}, t_i\right)$, is obtained as

$$\beta_i = \left\|\left(\overline{U}_i, \overline{V}\right)\right\| \tag{34}$$

where $(\overline{U}_i, \overline{V})$ is the most probable point of the i-th performance function $g^*\left(\boldsymbol{U}_i, \boldsymbol{V}, t_i\right)$.

Using the first-order Taylor series to expand the functional function $g^*\left(\boldsymbol{U}_i, \boldsymbol{V}, t_i\right)$ at the most probable point, the reliability calculation equation of the approximate performance function is obtained as

$$P_s(T) = P\left\{\bigcap_{i=1}^{m} \beta_i + \boldsymbol{\alpha}_{U,i}\boldsymbol{U}_i^T + \boldsymbol{\alpha}_{V,i}\boldsymbol{V}^T > 0\right\} \tag{35}$$

where $\boldsymbol{\alpha}_{U,i} = \frac{\overline{U}_i}{\beta_i}$ and $\boldsymbol{\alpha}_{V,i} = \frac{\overline{V}}{\beta_i}$ are the gradient vectors of the random vector $\boldsymbol{U}_i$ and $\boldsymbol{V}$, respectively.

Let $L_i = \beta_i + \boldsymbol{\alpha}_{U,i}\boldsymbol{U}_i^T + \boldsymbol{\alpha}_{V,i}\boldsymbol{V}^T$. Since the transformed random vectors $\boldsymbol{U}_i$ and $\boldsymbol{V}$ are independent standard normal distribution vectors, L_i obeys a normal distribution with the expected value $\mu_i = \beta_i$ and the standard deviation $\sigma_i = 1$. Considering that the time-variant wear quantity function is equivalent to a Gaussian process, the correlation coefficient between random variables is obtained as

$$\rho_{i,j} = \frac{Cov\left(L_i, L_j\right)}{\sigma_{L_i}\sigma_{L_j}} = Cov\left(L_i, L_j\right) = \sum_{k=1}^{m} \alpha_{U,i,k}\alpha_{U,j,k}C_k\left(t_i, t_j\right) + \boldsymbol{\alpha}_{V,i}^T\boldsymbol{\alpha}_{V,j} \tag{36}$$

where $C_k(\cdot)$ represents the autocorrelation function of time-variant parameter $X_k(t)$.

Let the correlation coefficient matrix $\boldsymbol{\rho}=\left[\rho_{i,j}\right]$. Thus, using the first-order second-moment method to solve Eq. (30), the precision reliability of the rotor-bearing system is obtained as

$$P_s(T) = \Phi_m(\boldsymbol{\beta}, \boldsymbol{\rho}) \tag{37}$$

5 Case investigations

In this section, a numerical control rotary table is taken as an example to elaborate the proposed method in detail, as shown in Fig. 9. The rotary table is composed of the gear MAU, the worm shaft MAU, and the worktable MAU. The gear MAU provides power input, the worm shaft MAU transmits motion and power, and the worktable MAU realizes the function of indexing and positioning.

As shown in Fig. 10, the wear of the worktable MAU mainly occurs from the worm wheel and bearing. The structural parameters of the worm wheel are listed in Table 1; the structural parameters of the bearing are listed in Table 2.

According to Eqs. (3)–(6), the time-variant wear (μm/h) of the worm wheel is calculated as

$$\Delta e_g^{(w)I}(t) = 0.034707t$$

According to Eqs. (9)–(18), the time-variant wear (μm/h) of the bearing is calculated as

$$\Delta e_p^{(w)O}(t) = 0.0005063t$$

Generally, the initial random errors of the components are subject to normal distribution within the tolerance range. The distribution information of the random errors affecting spatial pose errors of the power output part during the worktable MAU assembly process are listed in Table 3.

The values of each random error are obtained by Monte Carlo simulation method [37]. Substituting these values into

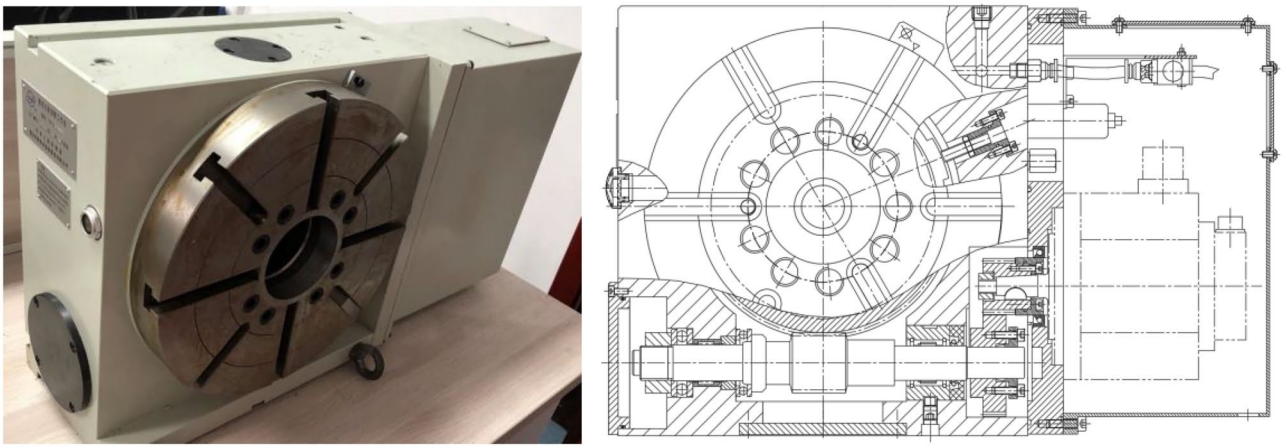

Fig. 9 The numerical control rotary table

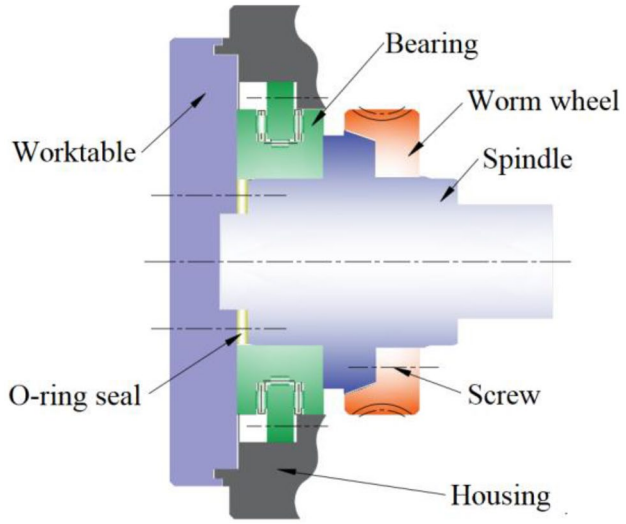

Fig. 10 The structure of the worktable MAU

Eqs. (22–24), the spatial pose errors of the power input part and the power output part are calculated. The fitting joint distribution of error components in each degree of freedom can be obtained with enough sampling times. The combined distribution of the eccentric error of the worm wheel and worktable is as follows:

$$\Delta e_{ip}^{(w)I} \sim N\left(4.25, 2.25^2\right), \Delta e_{ip}^{(w)O} \sim N\left(28.25, 6.80^2\right)$$

The geometric characteristic error distribution of the worm wheel is listed in Table 4:

According to the model in Sect. 3, the indexing precision of the worktable MAU is calculated as

$$\begin{aligned}\Delta e^{(w)}(t)=&\Delta e_{ig}^{(w)I} + 0.5\Delta f_{ic}^{'(w)I} \sin(2\pi\omega^{(w)}t) + 0.5\Delta F_{ic}^{'(w)I} \sin(2\pi\omega^{(w)}t)+\\ &0.034707t + \Delta e_{ip}^{(w)I} \sin\left(2\pi\omega^{(w)}t + \beta^{(w)I} + \alpha^{(w)}\right)+\\ &\left(\Delta e_{ip}^{(w)O} + 0.0005063t\right) \sin\left(2\pi\omega^{(w)}t + \beta^{(w)O} + \alpha\right)\end{aligned}$$

Similarly, the indexing precision of the worm shaft MAU is calculated as

$$\begin{aligned}\Delta e^{(s)}(t)=&\Delta e_{ig}^{(s)I} + 2.9264\times10^{-5}t + 0.5\Delta f_{ic}^{'(s)I} \sin(2\pi\omega^{(s)}t) + 0.5\Delta F_{ic}^{'(s)I} \sin(2\pi\omega^{(s)}t)+\\ &\Delta e_{ip}^{(s)I} \sin\left(2\pi\omega^{(s)}t + \beta^{(s)I} + \alpha^{(s)I}\right) + \Delta e_{ig}^{(s)O} + \Delta e_{is}^{(s)O}+\\ &\left(\Delta e_{ip}^{(s)O} + 0.0167t\right) \sin\left(2\pi\omega^{(s)}t + \beta^{(s)O} + \alpha^{(s)O}\right)\end{aligned}$$

The probability distributions of random variables in worm shaft MAU are listed in Table 5.

The indexing precision of the gear MAU is calculated as

$$\begin{aligned}\Delta e^{(g)}(t)=&\Delta e_{ig}^{(g)O} + 5.8528\times10^{-5}t + 0.5\Delta f_{ic}^{'(g)O} \sin(2\pi\omega^{(g)}t) + 0.5\Delta F_{ic}^{'(g)O} \sin(2\pi\omega^{(g)}t)+\\ &+\Delta e_{ip}^{(g)O} \sin\left(2\pi\omega^{(g)}t + \beta^{(g)O} + \alpha^{(g)}\right)\end{aligned}$$

Table 1 Structural parameters of the worm wheel

Item	Value	Item	Value
Poisson ratio	0.33	Axial module	2.25
Elastic modulus	1.19×10^{11} N/m.^{2}	Surface roughness	1.6 μm
Viscosity-pressure coefficient of lubricant	1.6819×10^{-8} m.^{2}/N	Base radius	0.10125 m
Torque	180 N·m	Face width	0.036 m
Speed	11.1 r/min	Pressure angle	15°

The probability distributions of random variables in gear MAU are listed in Table 6.

The indexing precision of the rotary table is calculated as

$$\Delta e(t) = \Delta e^{(w)}(t) + \Delta e^{(s)}(t) + \Delta e^{(g)}(t)$$

Considering that the output precision of the servo motor is generally fixed, the allowable indexing precision value after subtracting the servo motor precision is $\Delta e^* = 80\mu m$. The numerical analysis is carried out according to the method in Sect. 4. According to the simulation results shown in Fig. 11, when the NC rotary table has been operating for 930 h, its kinematic precision reliability begins to decrease. The confidence interval is generally 95%; when the operation time reaches 1255 h, the kinematic precision reliability is reduced to 0.95. One thousand two hundred fifty-five hours is considered as the precision life limit of the rotary table, and maintenance is required. In comparison with the expected 1200-h precision life, it can be determined that the precision design of the NC turntable is reasonable and the proposed evaluation model is effective. As demonstrated in the figure, the curve is gentle at the initial stage of kinematic precision reliability decline, and the precision reliability decreases significantly when reaching the precision limit. This is also identical with the actual operation situation. Consequently, it shows that this method can accurately predict the precision life of the rotary table in the design stage.

Further, we investigate the influence of different wear resistances of component materials on the kinematic precision life of the rotary table. From the calculation results, it

Table 2 Structural parameters of the bearing

Item	Value	Item	Value
Poisson ratio of the inner raceway material	0.288	Poisson ratio of the roller material	0.3
Elastic modulus of the inner raceway material	2.06×10^{11} N/m.^{2}	Elastic modulus of the roller material	2.08×10^{11} N/m.^{2}
Poisson ratio of the outer raceway material	0.28	Length of the roller	14 mm
Elastic modulus of the outer raceway material	2.10×10^{11} N/m.^{2}	Diameter of the center circle	153 mm
Friction torque	7 N·m	Number of rollers	50

Table 3 Distribution information of each random error/μm

Mating type	Error	Tolerance range	Distribution parameters
Bearing cylindrical fit with the spindle and box	Diameter of the spindle	[−10,0]	$N(-5,1.34.^2)$
	Diameter of the box hole	[0,100]	$N(50,12.25.^2)$
Bearing planar fit with the spindle	Flatness of the spindle shoulder	[0,5]	$N(2.5,0.86.^2)$
Spindle cylindrical fit with the worktable	Diameter of the spindle	[−22,0]	$N(-11,2.88.^2)$
	Diameter of the worktable hole	[0,35]	$N(17.5,4.52.^2)$
	Concentricity of the spindle	[0,10]	$N(5,2.12.^2)$
Worktable planar fit with the bearing	Perpendicularity of the worktable	[0,5]	$N(2.5,0.82.^2)$
	Flatness of the worktable	[0,5]	$N(2.5,0.82.^2)$
Worm wheel cylindrical fit with the spindle	Diameter of the spindle	[−18,0]	$N(-9,2.36.^2)$
	Concentricity of the spindle	[0,10]	$N(5,2.25.^2)$
	Diameter of the worm wheel hole	[0,25]	$N(12.5,3.1.^2)$
Worm wheel planar fit with the spindle	Perpendicularity of the worm wheel face	[0,10]	$N(5,2.25.^2)$

Table 4 The geometric characteristic error distribution of the worm wheel

Error	Distribution type	Distribution parameters
Tooth-to-tooth tangential composite error $\Delta f_{ic}^{'(w)I}$/μm	Rayleigh distribution	$R(1.2)$
Total tangential composite error $\Delta F_{ic}^{'(w)I}$/μm	Rayleigh distribution	$R(2.6)$
Tooth thickness error caused by manufacturing $\Delta e_{ig}^{(w)I}$/μm	Normal distribution	$N(0,5.72.^2)$
Initial phase angle of eccentricity error $\beta^{(w)}$/rad	Uniform distribution	$U(0,2\pi)$

Table 5 The probability distributions of random variables in worm shaft MAU

Error	Distribution type	Distribution parameters
Tooth-to-tooth tangential composite error of gear $\Delta f_{ic}^{'(s)I}$/μm	Rayleigh distribution	$R(11)$
Total tangential composite error of gear $\Delta F_{ic}^{'(s)I}$/μm	Rayleigh distribution	$R(13)$
Tooth thickness error of gear caused by manufacturing $\Delta e_{ig}^{(s)I}$/μm	Normal distribution	$N(0,2.15.^2)$
Eccentric error of gear caused by assembling $\Delta e_{ip}^{(s)I}$/μm	Normal distribution	$N(4.5,1.28.^2)$
Profile form error of worm shaft $\Delta e_{is}^{(s)O}$/μm	Rayleigh distribution	$R(3.55)$
Tooth thickness error of worm shaft caused by manufacturing $\Delta e_{ig}^{(s)O}$/μm	Normal distribution	$N(0,4.36.^2)$
Eccentric error of worm shaft caused by assembling $\Delta e_{ip}^{(s)O}$/μm	Normal distribution	$N(1.75,1.04.^2)$
Initial phase angle of eccentricity error $\beta^{(s)}$/rad	Uniform distribution	$U(0,2\pi)$

Table 6 The probability distributions of random variables in gear MAU

Error	Distribution type	Distribution parameters
Tooth-to-tooth tangential composite error $\Delta f_{ic}^{\prime(g)O}$/μm	Rayleigh distribution	$R(10)$
Total tangential composite error $\Delta F_{ic}^{\prime(g)O}$/μm	Rayleigh distribution	$R(10)$
Tooth thickness error caused by manufacturing $\Delta e_{ig}^{(g)O}$/μm	Normal distribution	$N(0,1.32.^2)$
Eccentric error caused by assembling $\Delta e_{ip}^{(g)O}$/μm	Normal distribution	$N(11.25,3.02.^2)$
Initial phase angle of eccentricity error $\beta^{(g)}$/rad	Uniform distribution	$U(0,2\pi)$

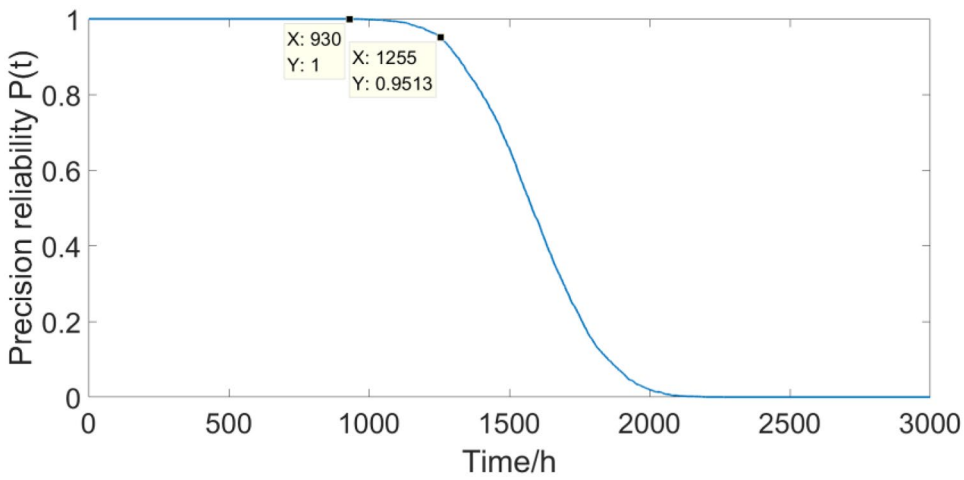

Fig. 11 Kinematic precision reliability of the rotary table with multi-source wears and random errors

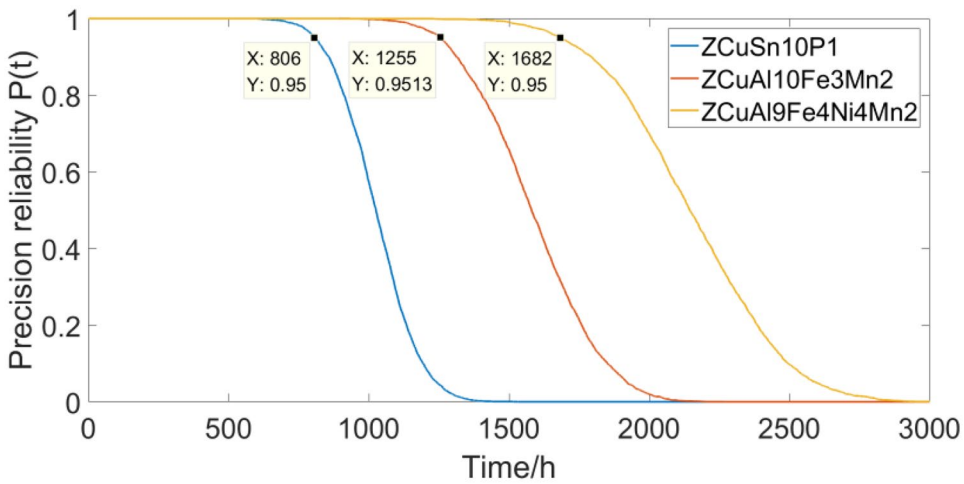

Fig. 12 Effects of the material type on the kinematic precision reliability

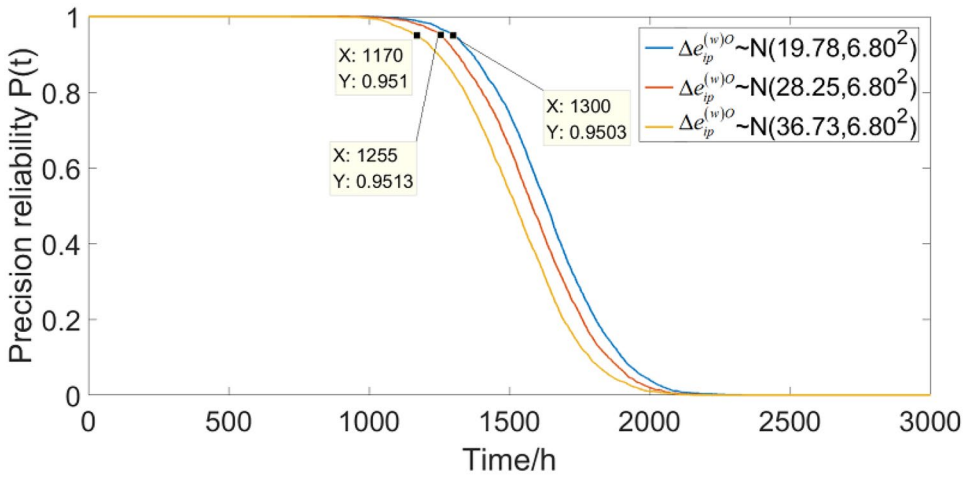

Fig. 13 Effects of the tolerance range on the kinematic precision reliability

indicates that the main wears locate on the worm wheel of the NC rotary table. Therefore, three different grades of copper are selected for simulation. Based on the results shown in Fig. 12, when ZCuSn10P1 is selected as the worm wheel material, the precision life of the rotary table is 806 h. When ZCuAl10Fe3Mn2 is used, the precision life increases by 449 h. When the worm wheel is made of the ZCuAl9Fe4Ni4Mn2, the precision life is further improved to 1682 h. Combined with the conversion cost of each material and the maintenance cost of the rotary table, the material selection in the design stage can be realized.

Different tolerance ranges of components also have an impact on the kinematic precision reliability. In order to reveal the influence, the assembly errors of the worm wheel are taken as an example; different distribution ranges of the worm wheel eccentric error are selected for simulation. According to the results shown in Fig. 13, when $\Delta e_{ip}^{(w)O} \sim N\left(19.78,\ 6.80^2\right)$, the manufacturing error of the components is smaller, and the precision life of the rotary table increases to 1300 h. When $\Delta e_{ip}^{(w)O} \sim N\left(36.73,\ 6.80^2\right)$, this indicates that the manufacturing quality is relatively poor and leads to a reduction in precision life to 1170 h. Thus, the tolerance optimization design can be realized according to the precision demand and cost.

6 Conclusions

In this paper, a practical and effective approach for kinematic precision reliability evaluation of rotor-bearing systems is proposed innovatively. This method has advantages in the quantity of error terms and the accuracy of assessment results, and can be provided with great application potential in precision design and maintenance strategy for rotor-bearing systems. The study contains the following:

1. A comprehensive kinematic precision model describing the mapping relationship from component geometric errors to the system output precision is proposed based on the meta-action theory and screw theory, and it can overcome the limitations of the traditional methods in the number of error sources.
2. Both the initial errors conforming to specified random distributions and the time-dependent wears are contained in the precision reliability function of rotor-bearing systems; a kinematic precision reliability evaluation model with multiple error sources for rotor-bearing systems is provided by introducing the stochastic process discretization method.
3. An example for a numerical control rotary table is investigated to demonstrate the effectiveness of this approach. The simulation results obtained by changing the parameters of error sources show that the proposed method is practical and helpful to increase the precision reliability of rotor-bearing systems in the design phase.

However, this method only calculates the wear errors among the time-variant error sources; some random errors affected by changeable environmental factors during the operation of rotor-bearing systems also need to be seriously considered, such as thermal errors, deformation errors caused by residual stress release, and runout errors caused by fastener loosening. In addition, different lubrication states will affect the wear rate, and the fatigue wear is also an important constituent part in the wear of gears. The influence of the above-mentioned factors on the kinematic precision reliability of the systems will be comprehensively taken into consideration in our future investigations.

Author contribution All authors contributed to the study conception and design. Material preparation, data collection, and analysis were performed by Hongwei Wang, Jiawei Xiang, and Yulong Li. The first draft of the manuscript was written by Hongwei Wang, and all authors

commented on previous versions of the manuscript. All authors read and approved the final manuscript.

Funding This work was supported by the National Natural Science Foundation of China (No. U1909217), the Zhejiang Natural Science Foundation of China (No. LD21E050001), and the Wenzhou Major Science and Technology Innovation Project of China (No. ZG2021019, ZG2021027).

Declarations

Competing interests The authors declare no competing interests.

References

1. Sukhija RP, Rao AC (1986) Mechanical error synthesis of path generating mechanisms using reliability index. T Can Soc Mech Eng 10(2):85–90
2. Kong XF, Yang J, Hao SH (2021) Reliability modeling-based tolerance design and process parameter analysis considering performance degradation. Reliab Eng Syst Safe 207:107343
3. Tavangar M, Hashemi M (2022) Reliability and maintenance analysis of coherent systems subject to aging and environmental shocks. Reliab Eng Syst Safe 218:108170
4. Tang H, Duan JA, Lan SH, Shui HY (2015) A new geometric error modeling approach for multi-axis system based on stream of variation theory. Int J Mach Tools Manuf 92:41–51
5. Yang JX, Ding H (2016) A new position independent geometric errors identification model of five-axis serial machine tools based on differential motion matrices. Int J Mach Tools Manuf 104:68–77
6. Bozca M (2018) Transmission error model-based optimisation of the geometric design parameters of an automotive transmission gearbox to reduce gear-rattle noise. Appl Acoust 130:247–259
7. Liu Y, Wan M, Xiao QB, Zhang WH (2019) Identification and compensation of geometric errors of rotary axes in five-axis machine tools through constructing equivalent rotary axis (ERA). Int J Mech Sci 152:211–227
8. Yang WJ, Liu XJ, Guo XT, Lu WL, Yao ZJ, Lei ZL (2021) A method for simultaneously measuring 6DOF geometric motion errors of a precision rotary stage based on absolute position-distance measurement. Opt Laser Eng 138:106420
9. Wang K, Zhou CG, Ou Y, Feng HT (2022) Investigation of the transmission accuracy of ball screw considering errors and preloading level. Int J Adv Manuf Technol 118:3917–3932
10. Zhang GB, Lou JH, Li DY, Peng L (2015) Fault diagnosis study of complex mechanism based on FMA function decomposition model. Procedia CIRP 27:176–180
11. Yu H, Zhang GB, Ran Y, Li MQ, Jiang DX, Chen YQ (2020) A reliability allocation method for mechanical product based on meta-action. IEEE T Reliab 69(1):373–381
12. Wang ZC, Ran Y, Yu H, Jin CX, Zhang GB (2021) Failure mode and effects analysis using function–motion–action decomposition method and integrated risk priority number for mechatronic products. Qual Reliab Eng Int 37(6):2875–2899
13. Wang ZC, Ran Y, Yang X, Li XL, Chen YF, Zhang GB (2021) Primary failure mode and effects analysis with function-motion-action hierarchy structure for mechatronic systems. Eng Fail Anal 130:105775
14. Mu ZY, Ran Y, Zhang GB, Wang HW, Yang X (2021) Remaining useful life prediction method for machine tools based on meta-action theory. P I Mech Eng O-J Ris 235(4):580–590. https://doi.org/10.1177/1748006X211002544
15. Chen YF, Ran Y, Wang ZC, Li XL, Yang X, Zhang GB (2021) Meta-action reliability-based mechanical product optimization design under uncertainty environment. Eng Appl Artif Intel 100:104174
16. Yang X, Ran Y, Zhang GB, Wang HW, Mu ZY, Zhi SG (2022) A digital twin-driven hybrid approach for the prediction of performance degradation in transmission unit of CNC machine tool. Robot Cim-Int Manuf 73(1):102230
17. Xiao LM, Huang GQ, Zhang GB (2022) Toward an action-granularity-oriented modularization strategy for complex mechanical products using a hybrid gga-cga method. Neural Comput Appl 34(8):6453–6487
18. Huang XZ, Hu S, Zhang YM, Xu YC (2015) A method to determine kinematic accuracy reliability of gear mechanisms with truncated random variables. Mech Mach Theory 92:200–212
19. Cai LG, Zhang ZL, Cheng Q, Liu ZF, Gu PH, Qi Y (2016) An approach to optimize the machining accuracy retainability of multi-axis NC machine tool based on robust design. Precis Eng 43:370–386
20. Wang W, Zhang YM, Li CY (2017) Dynamic reliability analysis of linear guides in positioning precision. Mech Mach Theory 116:451–464
21. Zhang ZL, Liu ZF, Cai LG, Cheng Q, Qi Y (2017) An accuracy design approach for a multi-axis NC machine tool based on reliability theory. Int J Adv Manuf Technol 91(5–8):1547–1566
22. Yang X, Ran Y, Wang ZC, Mu ZY, Zhang GB (2021) Early prediction method for assembly precision of mechanical system and assessment of precision reliability. Int J Adv Manuf Technol 112:203–220
23. Ma XX, Zhang ZG, Hua HX (2022) Uncertainty quantization and reliability analysis for rotor/stator rub-impact using advanced Kriging surrogate model. J Sound Vib 525:116800
24. Wang W, Shen G, Zhang YM, Zhu ZC, Li CY, Lu H (2021) Dynamic reliability analysis of mechanical system with wear and vibration failure modes. Mech Mach Theory 163:104385
25. Chen JH, Chen LM, Qian LF, Chen GS, Zhou SJ (2022) Time-dependent kinematic reliability analysis of gear mechanism based on sequential decoupling strategy and saddle-point approximation. Reliab Eng Syst Safe 220:108292
26. Jiang S, Li W, Xin GF, Sheng LC, Wang YQ (2022) Study on dynamic reliability of permanent magnet gear transmission system with wear and failure correlation. Eng Fail Anal 131:105802
27. Zhang XG, Li YL, Ran Y, Zhang GB (2020) Stochastic models for performance analysis of multistate flexible manufacturing cells. J Manuf Syst 55:94–108
28. Pan ZQ, Balakrishnan N (2011) Reliability modeling of degradation of products with multiple performance characteristics based on gamma processes. Reliab Eng Syst Safe 96(8):949–957
29. Cheng YW, Zhu HP, Hu K, Wu J, Shao XY, Wang YH (2019) Reliability prediction of machinery with multiple degradation characteristics using double-Wiener process and Monte Carlo algorithm. Mech Syst Signal Pr 134:106333
30. Andrieu-Renaud C, Sudret B, Lemaire M (2004) The PHI2 method: a way to compute time-variant reliability. Reliab Eng Syst Safe 84(1):75–86
31. Moura MDC, Zio E, Lins ID, Droguett E (2011) Failure and reliability prediction by support vector machines regression of time series data. Reliab Eng Syst Safe 96(11):1527–1534
32. He JJ, Huang M, Wang W, Wang SH, Guan XF (2021) An asymptotic stochastic response surface approach to reliability assessment under multi-source heterogeneous uncertainties. Reliab Eng Syst Safe 215:107804
33. Jiang C, Qiu HB, Gao L, Wang DP, Yang Z, Chen LM (2020) Real-time estimation error-guided active learning Kriging

method for time-dependent reliability analysis. Appl Math Model 77(1):82–98
34. Janakiraman V, Li S, Kahraman A (2014) An investigation of the impacts of contact parameters on wear coefficient. J Tribol 136(3):69–74
35. Jiang C, Huang XP, Wei XP, Liu NY (2017) A time-variant reliability analysis method for structural systems based on stochastic process discretization. Int J Mech Mater Des 13:173–193. https://doi.org/10.1007/s10999-015-9324-z
36. Lebrun R, Dutfoy A (2009) An innovating analysis of the Nataf transformation from the viewpoint of copula. Probabilist Eng Mech 24(3):312–320
37. Zhang ZL, Cheng Q, Qi BB, Tao ZQ (2021) A general approach for the machining quality evaluation of S-shaped specimen based on POS-SQP algorithm and Monte Carlo method. J Manuf Syst 60:553–568